

# Cosattering in the Extended Singlet-Scalar Higgs Portal

---

Bastián Díaz Sáez,<sup>a,b</sup> Jayita Lahiri,<sup>c</sup> Kilian Möhling<sup>d</sup>

<sup>a</sup>*Instituto de Física, Pontificia Universidad Católica de Chile, Avenida Vicuña Mackenna 4860, Santiago, Chile*

<sup>b</sup>*Millennium Institute for Subatomic Physics at the High-Energy Frontier (SAPHIR), Fernández Concha 700, Santiago, Chile*

<sup>c</sup>*II. Institut für Theoretische Physik, Universität Hamburg, Luruper Chaussee 149, 22761 Hamburg, Germany*

<sup>d</sup>*Institut für Kern- und Teilchenphysik, TU Dresden, Zellescher Weg 19, 01069 Dresden, Germany*  
*E-mail:* [bastian.diaz@uc.cl](mailto:bastian.diaz@uc.cl), [jlahiri29@gmail.com](mailto:jlahiri29@gmail.com),  
[kilian.moehling@tu-dresden.de](mailto:kilian.moehling@tu-dresden.de)

**ABSTRACT:** We study the coscattering mechanism in a simple Higgs portal which add two real singlet scalars to the Standard Model. In this scenario, the lighter scalar is stabilized by a single  $Z_2$  symmetry and acts as the dark matter relic, whose freeze-out is driven by conversion processes. The heavier scalar becomes an unstable state which participate actively in the coscattering. We find viable parameter regions fulfilling the measured relic abundance, while evading direct detection and big-bang nucleosynthesis bounds. In addition, we discuss collider prospects for the heavier scalar as a long-lived particle at present and future detectors.

---

## Contents

<b>1</b>	<b>Introduction</b>	<b>1</b>
<b>2</b>	<b>Model</b>	<b>2</b>
<b>3</b>	<b>Coscaterring or Conversion-driven freeze-out</b>	<b>2</b>
3.1	Boltzmann equations	3
3.2	Relic abundance	4
<b>4</b>	<b>Phenomenology</b>	<b>8</b>
4.1	Constraints	9
4.1.1	Direct detection	9
4.1.2	BBN	9
4.2	Long-lived particles	10
<b>5</b>	<b>Conclusions</b>	<b>11</b>
<b>A</b>	<b>Lagrangian original basis</b>	<b>12</b>
<b>B</b>	<b>Dark Matter Conversion Rate</b>	<b>12</b>
<b>C</b>	<b>Treatment of Radiative Corrections</b>	<b>14</b>

---

## 1 Introduction

Coscaterring [1] or Conversion-driven freeze-out [2] is a thermal dark matter (DM) framework in which the dark matter relic abundance is determined by the freeze-out of inelastic conversions in the dark sector. In the typical coannihilation regime such processes are assumed to be rapid enough to keep the dark sector in chemical equilibrium (CE) even long after the freeze-out of the DM from the thermal plasma. In contrast, in the coscaterring scenario the dark sector falls out of CE roughly once the conversion rates drop below the Hubble expansion rate. For previous studies of this mechanism in several different models see Refs. [3–13].

A typical feature of the coscaterring regime is the presence of long-lived particles (LLP), because the small coupling strength between the relic and unstable dark partner required for a fast freeze-out of the conversions in turn implies a narrow decay width of the dark partner. Furthermore, the masses of the DM species must be highly degenerate,  $\Delta m \ll m_{DM}$ , as otherwise the Boltzmann suppression of the conversion rate leaves the coscaterring mechanism inactive. Since the LLPs can couple much more strongly to the SM they are excellent candidates for direct detection of DM at present or future colliders [13–15].

In this paper, we study the coscattering mechanism in one of its perhaps simplest possible realizations, a two real singlet-scalar model coupling to the SM through the Higgs portal [16, 17]. Here, the lighter scalar is stabilized by a discrete  $\mathcal{Z}_2$  symmetry, while the second scalar acts as the unstable dark partner. We find that the coscattering regime allows for DM masses at the EW scale, while the dark partner constitutes a LLP with  $c\tau \lesssim 10^5$  km.

The paper is structured in the following way. In Sec. 2 we present the model. In Sec. 3 we discuss the calculation of the relic abundance in its different regimes, paying special attention to the coscattering regime. In Sec. 4 we present the relevant experimental constraints and obtain results for the expected lifetimes of the LLP. Finally, we give some concluding remarks in Sec. 5.

## 2 Model

We consider the SM extended by two real singlet-scalars  $S_1$  and  $S_2$ .  $S_1$  is taken to be the lighter scalar, which is stabilized by a  $Z_2$  symmetry under which  $S_i \rightarrow -S_i$ , while the SM fields transform trivially [16, 17]. As a result, the scalars couple to the SM only via the Higgs field. The corresponding Lagrangian in the scalar mass basis (for more details see App. A) is given by

$$\begin{aligned} \mathcal{L} = \mathcal{L}_{SM} + \sum_{i=1,2} \left( \frac{1}{2} (\partial_\mu S_i)^2 - \frac{m_i^2}{2} S_i^2 - \lambda_{i4} S_i^4 \right) - \lambda_{22} S_1^2 S_2^2 - \lambda_{13} S_1 S_2^3 - \lambda_{31} S_1^3 S_2 \\ - (\lambda_{H1} S_1^2 + \lambda_{H2} S_2^2 + \lambda_{12} S_1 S_2) \left( |H|^2 - \frac{v_h^2}{2} \right), \end{aligned} \quad (2.1)$$

where  $H$  denotes the SM Higgs doublet and  $v_h \approx 246$  GeV the Higgs vacuum expectation value (vev). None of the new scalars acquire a vacuum expectation value.

In the following, we consider  $(m_1, m_2, \lambda_{H1}, \lambda_{12}, \lambda_{H2}, \lambda_{22})$  the set of independent model parameters and denote the mass difference between the scalars by  $\Delta m \equiv m_2 - m_1 > 0$ . In the coscattering regime, the couplings  $\lambda_{13}$  and  $\lambda_{31}$  play a similar role to  $\lambda_{22}$  and are omitted for simplicity.

## 3 Coscattering or Conversion-driven freeze-out

In the coscattering regime we explicitly do not assume CE within the dark sector during the evolution of the DM number densities  $n_i$  up to the point of freeze-out. As a result, the full coupled Boltzmann equations (cBE), assuming all possible interaction terms, have to be solved in order to obtain the correct DM relic abundance. In the following we introduce  $x = m_1/T$  together with the typical definition of the DM yield  $Y_i := n_i/s$ , where  $s$  denotes the entropy density.

### 3.1 Boltzmann equations

The cBE for  $Y_1$  and  $Y_2$  reads

$$\begin{aligned} \frac{dY_1}{dx} = \frac{1}{3H} \frac{ds}{dx} & \left[ \langle \sigma_{1100} v \rangle (Y_1^2 - Y_{1e}^2) + \langle \sigma_{1200} v \rangle (Y_1 Y_2 - Y_{1e} Y_{2e}) \right. \\ & \left. + \langle \sigma_{1122} v \rangle \left( Y_1^2 - Y_2^2 \frac{Y_{2e}^2}{Y_{1e}^2} \right) + \frac{\Gamma_{1 \rightarrow 2}}{s} \left( Y_1 - Y_2 \frac{Y_{1e}}{Y_{2e}} \right) + \frac{\Gamma_2}{s} \left( Y_2 - Y_1 \frac{Y_{2e}}{Y_{1e}} \right) \right], \end{aligned} \quad (3.1a)$$

$$\begin{aligned} \frac{dY_2}{dx} = \frac{1}{3H} \frac{ds}{dx} & \left[ \langle \sigma_{2200} v \rangle (Y_2^2 - Y_{2e}^2) + \langle \sigma_{1200} v \rangle (Y_1 Y_2 - Y_{1e} Y_{2e}) \right. \\ & \left. - \langle \sigma_{1122} v \rangle \left( Y_1^2 - Y_2^2 \frac{Y_{2e}^2}{Y_{1e}^2} \right) - \frac{\Gamma_{1 \rightarrow 2}}{s} \left( Y_1 - Y_2 \frac{Y_{1e}}{Y_{2e}} \right) - \frac{\Gamma_2}{s} \left( Y_2 - Y_1 \frac{Y_{2e}}{Y_{1e}} \right) \right], \end{aligned} \quad (3.1b)$$

where  $H$  denotes the Hubble rate, 0 stand for any SM particles, and 1, 2 for  $S_1$  and  $S_2$  respectively. The equilibrium yields are given by

$$Y_{1e}(x) = \frac{45}{4\pi^4} \frac{x^2}{g_{*S}(x)} K_2(x), \quad (3.2a)$$

$$Y_{2e}(x) = \frac{45}{4\pi^4} \frac{x^2}{g_{*S}(x)} \frac{m_2^2}{m_1^2} K_2\left(\frac{m_2}{m_1} x\right), \quad (3.2b)$$

where  $K_2(x)$  is the modified Bessel function of the second kind,  $g_{*S}(x)$  the number of effective degrees of freedom associated to the entropy density  $s = \frac{2\pi^2}{45} g_{*S}(T) T^3$ . In contrast to the cBE for coannihilation, eqs. (3.1) explicitly contains the DM conversion rate

$$\Gamma_{1 \rightarrow 2} = \sum_{k,l} \langle \sigma_{1k \rightarrow 2l} v \rangle n_{k,e}, \quad (3.3)$$

where  $k$  and  $l$  denote light SM states. The calculation of the relevant conversion cross sections together with their thermal average is presented in App. B. The second important conversion process is given by decays of the unstable partner  $S_2$  with the thermally averaged decay rate [2]

$$\Gamma_2 \equiv \frac{K_1(m_2/T)}{K_2(m_2/T)} \sum_X \Gamma(2 \rightarrow X). \quad (3.4)$$

We solve the above cBE using `micrOMEGAs` 5.3.41 [18, 19], considering three separate sectors: i) the SM, ii) the DM candidate  $S_1$ , and iii) a dark sector for  $S_2$ . `micrOMEGAs` solves all the relevant average cross sections, including the two and three-body decay widths of  $S_2$  considering Lorentz time effects. To quantify the impact of rescattering and compare the results obtained from the full cBE to the results assuming CE we use [19]

$$\Delta_{1s}^\Omega \equiv 1 - \frac{\Omega h^2(1 \text{ sector})}{\Omega h^2(2 \text{ sectors})}, \quad (3.5)$$

where  $\Omega h^2(1 \text{ sector})$  is obtained using the `darkOmega` function of `micrOMEGAs` and  $\Omega h^2(2 \text{ sectors})$  is obtained from `darkOmegaN`<sup>1</sup>. The scaling of each process with the model parameters are listed in Table 1.

<sup>1</sup>In the present paper we did not make explicit use of the function  $\Delta_{2s}^\Omega$  defined in [19], although part of the analysis in this section contemplates the information that could be obtained with that function.

Initial	Final	Scaling
1 1	0 0	$\lambda_{H1}^2, \lambda_{12}^2$
2 2	0 0	$\lambda_{H2}^2, \lambda_{12}^2$
1 1	2 2	$\lambda_{H1}^2, \lambda_{12}^2, \lambda_{H2}^2, \lambda_{22}^2$
1 2	0 0	$\lambda_{H1}^2, \lambda_{12}^2, \lambda_{H2}^2$
1 0	2 0	$\lambda_{H1}^2, \lambda_{12}^2, \lambda_{H2}^2$
2	1 0	$\lambda_{12}^2$

**Table 1:** Scattering and decay processes with their corresponding scaling, ignoring the quartic couplings  $\lambda_{13}$  and  $\lambda_{31}$ .

### 3.2 Relic abundance

The basic characteristic of the conversion-driven freeze-out in the two scalar Higgs portal are:

1.  $S_1$  remains in CE with  $S_2$  only through either (inverse) decays or cospattering processes  $10 \leftrightarrow 20$ .
2. Annihilation processes  $S_1 S_i \rightarrow XX$  involving  $S_1$  can be neglected.

The first condition requires that  $\lambda_{12}$  is non-vanishing but small enough for the conversion processes not to surpass the Hubble expansion rate at  $T \lesssim m_1$ . On the other hand, to prevent an early freeze-out and overabundance of DM it is required that  $S_2$  couples strongly with the Higgs  $\lambda_{H2} \sim 1$ . The second condition is fulfilled only when in addition to  $\lambda_{12}$ , also  $\lambda_{H1} \ll 1$ . In case of on-shell (inverse) decays of  $S_2$ , the dark sector can stay in CE for much smaller couplings compared to the case of off-shell decays, however, we have checked that in both cases conversion-driven freeze-out is possible (in contrast to [1] who assumed that 2-body decays are forbidden). In the last part of this section we analyse this point in more detail. Lastly, we note that the contact interaction terms in eq. (2.1) can not be arbitrarily large, as otherwise they will recover CE between  $S_1$  and  $S_2$ . The impact of  $\lambda_{22}$ ,  $\lambda_{13}$  and  $\lambda_{31}$  is discussed in more detail at the end of this section. In Table 1 we show the parameter dependence for each process that enters in eqs. 3.1.

In order to simplify the discussion and exploration of the parameter space of the model in the cospattering framework, we define the *simplest benchmark scenario* (SBS) considering  $\lambda_{H1} = \lambda_{22} = 0$ , and the relevant parameters as

$$(m_1, m_2, \lambda_{H2}, \lambda_{12}). \quad (3.6)$$

Deviations from the SBS will be explicitly shown in some parts of the paper. As a warm up example of the features of cospattering in the SBS, in Fig. 1 we show a typical evolution of the DM yield in the cospattering regime fulfilling the correct relic abundance  $\Omega h^2 = 0.12$ , for  $(m_1, m_2) = (500, 505)$  GeV, and  $(\lambda_{12}, \lambda_{H2}) = (2.6 \times 10^{-5}, 1)$ . Notice that  $Y_1$  deviates

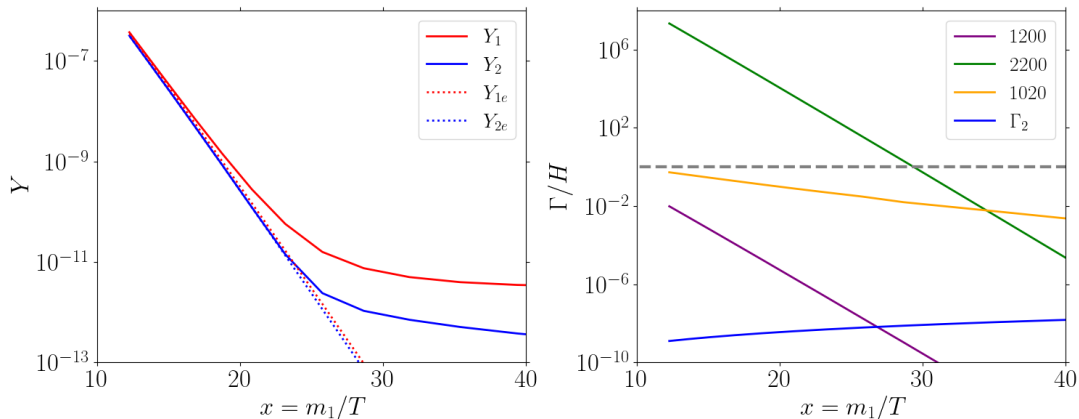


**Figure 1:** (left) Relic abundance in the cospattering regime for the benchmark point  $(m_1, m_2) = (500, 505)$  GeV,  $(\lambda_{12}, \lambda_{H2}) = (2.6 \times 10^{-5}, 1)$ . (right) Scattering and decay rates compared to the Hubble rate as a function of the inverse temperature at the benchmark point. The dashed horizontal line represents when the rate interactions equal the Hubble rate.

from its equilibrium already near  $x \approx 12$ , whereas  $Y_2$  stays in equilibrium for longer. This behavior is characteristic of the cospattering regime. In the right plot, we compare the reaction rates with the Hubble expansion, where  $\Gamma_{ij} \equiv \frac{\gamma_{ij \rightarrow kl}}{n_{1e}}$  and  $\gamma_{ij \rightarrow kl}$  denotes the reaction density. In particular it can be seen that the DM conversion rate 1020 (yellow line) drops below the Hubble expansion at the same time as  $S_1$  starts to freeze out from the thermal bath. Note that in the SBS scenario, decays and coannihilations are well below the Hubble rate and are completely negligible during the freeze-out process.

With this simple picture in mind, we now vary  $m_2$  and  $\lambda_{12}$  and study their impact on the relic abundance. We have performed a grid scan over  $\lambda_{12} \in [10^{-5}, 10]$  and  $m_2 \in [500, 630]$  GeV, keeping  $m_1 = 500$  GeV and  $\lambda_{H2} = 1$  fixed. The results are shown in Fig. 2, where the red curves correspond to the solutions of the full cBE obtained with `darkOmegaN`, the blue curves were obtained using `darkOmega` and the orange curves were obtained ignoring the conversion processes 1020. While the relic abundance shows a similar behavior when varying  $\lambda_{12}$  for different values of  $\Delta m$ , the predicted relic abundance differs very strongly. This is due to the fact that the effective annihilation rate determining the point of freeze-out  $e^{-2x\Delta m/m_1} \langle \sigma_{2200} v \rangle$  is exponentially suppressed for large  $\Delta m$ . This suppression leads to a smaller effective cross section which implies a faster freeze-out and larger relic abundance, as can be seen in Fig. 2.

As an example to better understand the dependence of  $\Omega h$  on  $\lambda_{12}$ , we consider the case  $\Delta m = 30$  GeV (dot-dashed line). In Fig. 2 we have highlighted three distinct regions for the behaviour of the relic abundance. The cospattering mechanism is only active in region I where  $\lambda_{12}$  is small enough so that the 1020 conversion processes freeze-out quickly. As the coupling increases, CE is recovered and the relic abundance becomes insensitive to  $\lambda_{12}$  in region II. In this case the relic abundance is mainly determined by  $S_2$  annihilation, which is also called *mediator freeze-out regime* [7]. Finally, in region III for  $\lambda_{12} \gtrsim 0.1$  coannihilations

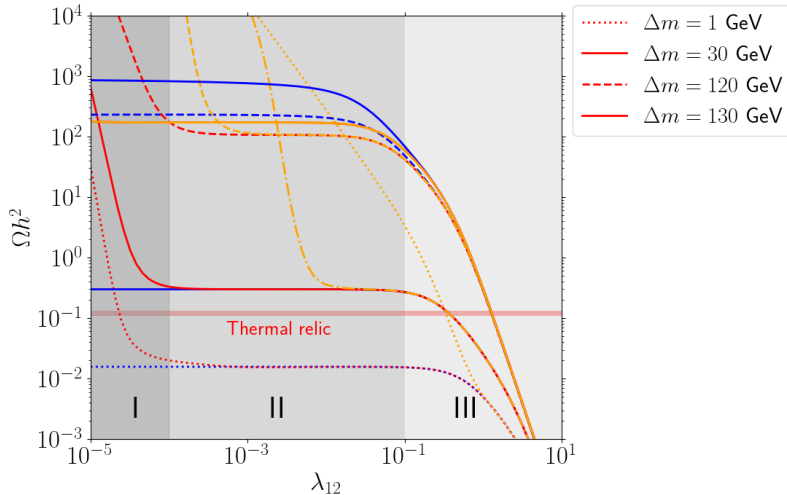


**Figure 2:** Relic abundance obtained in the SBS considering  $m_1 = 500$  GeV. The red curves are obtained with `darkOmegaN`, the blue ones with `darkOmega`, and the orange ones without considering the process 1020 in eqs. 3.1 (in `micrOMEGAs` this quantity can be obtained using the command "Excluding2010"). Note that the solid red curve is covered by the solid orange curve. The regions shown here as I, II and III correspond to the case of  $\Delta = 30$  GeV.

between  $S_1$  and  $S_2$  become relevant and the relic abundance again depends on  $\lambda_{12}$ .

For each  $\Delta m$  in Fig. 2 we have also included the corresponding relic abundance obtained from `darkOmegaN` when neglecting the processes 1020, but keeping decays<sup>2</sup>. The resulting abundances are plotted as the orange lines, highlighting the fact that for small values of  $\lambda_{12}$  decays are not able to support CE in the absence of processes of the type 1020. In the case of on-shell decays (solid orange), where the decay rates are much larger, CE is maintained also at small  $\lambda_{12}$ . In this case the orange and red lines overlap in the whole range of small couplings. We have also included the results for the relic abundance calculated using the function `darkOmega` of `micrOMEGAs` (blue lines). This function assumes that that CE between  $S_1$  and  $S_2$  is maintained during the entire evolution of the DM yield. In case of  $\Delta m = 1$  and 30 GeV, the relic abundance obtained with the functions `darkOmega` and `darkOmegaN` agree very well in regions II and III, indicating that CE is present. In case of  $\Delta m = 120$  GeV, the results assuming CE are larger by roughly a factor of two, which further increases for larger mass differences. We have checked that in these cases the rate of (inverse) decays remains above the Hubble expansion, ensuring CE. The correct relic abundance is therefore obtained from `darkOmega`, while `darkOmegaN` assumes separate CE of the different sectors, which is unrealistic, particularly when on-shell decays are present.

From the case with  $m_2 = 630$  GeV shown in Fig. 2, we have seen that on-shell decays maintain CE for much smaller  $\lambda_{12}$  values. To further illustrate this fact, in Fig. 3 (left) we show the early departure from CE of the yield  $Y_1$  in the off-shell case,  $m_2 = 620$  GeV,

<sup>2</sup>In `micrOMEGAs` this is achieved using the option `Excluding2010`.

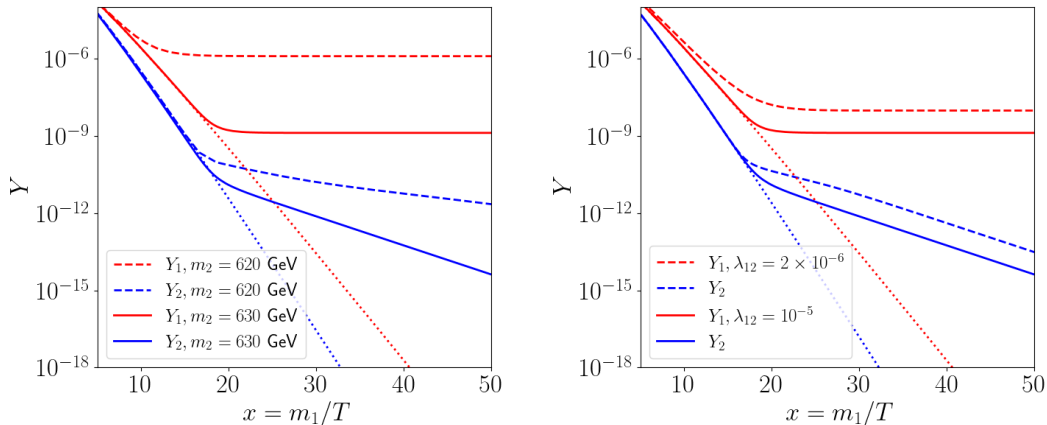


**Figure 3:** (left) DM yield evolution for the case of off-shell (dashed) and on-shell (solid) decays with  $m_1 = 500$  GeV,  $\lambda_{12} = 10^{-5}$ ,  $\lambda_{H2} = 1$ , and  $\lambda_{H1} = \lambda_{22} = 0$ . (right) DM yield evolution for on-shell decays for  $(m_1, m_2) = (500, 630)$  GeV, with  $\lambda_{12} = 2 \times 10^{-6}$  (dashed) and  $\lambda_{12} = 10^{-5}$  (solid).

compared to the on-shell case,  $m_2 = 630$  GeV, for a fixed value of  $\lambda_{12}$ . In Fig. 3 (right) we show that, once on-shell decays are present, small enough values of  $\lambda_{12}$  also break the CE<sup>3</sup>. In other words, as  $\Delta m$  increases, the relevance of decays in maintaining CE becomes stronger, requiring smaller  $\lambda_{12}$  for cospattering.

On the other hand, the contact terms proportional to the couplings  $\lambda_{22}, \lambda_{13}$  and  $\lambda_{31}$  can have a strong impact on the relic density. In particular, when they take sizable values, i.e. either  $\lambda_{22}, \lambda_{13}$  or  $\lambda_{31} \gtrsim 0.1$ , they bring  $S_1$  and  $S_2$  back into CE. To quantify this, in Fig. 4 (left) we show the effect of each separate coupling on the relic abundance for two set of masses. In each case, the value of  $\lambda_{12}$  was fixed in order to obtain the correct relic abundance by `darkOmegaN` in the limit of vanishing contact terms. As the contact couplings get sizable values, they start to affect the relic abundance calculation with `darkOmegaN` as they tend to establish partial CE between  $S_1$  and  $S_2$ . Once the contact couplings are big enough, the CE is established, such that the calculation using `darkOmega` and `darkOmegaN` agree with each other<sup>4</sup>. As we focus on the cospattering, we do not include deviations induced by the contact terms of this Higgs portal scenario, therefore in the rest of the paper we assume they are sufficiently small to not deviate from the relic abundance calculation with `darkOmegaN`.

To end this section, we comment about the low mass regime  $m_1 < m_h/2$ , which turns out to be disfavored by LHC data. From the above discussion we found that cospattering

<sup>3</sup>We have checked this in the case of on-shell decays, cospattering appears in the ballpark of  $\mathcal{O}(\lambda_{12}) \propto 10^{-6}$ , but as a strong overabundance is obtained in this parameter space region, we do not focus on this case in this paper.

<sup>4</sup>It is interesting to remark that for the case in which  $\lambda_{22}$  takes sizable values, and  $\lambda_{12}$  remains sufficiently small to not maintain CE between  $S_1$  and  $S_2$ , one recover the yield dynamic of two stable DM, known as assisted freeze-out [20] (also see [21, 22]). As in the present framework  $S_2$  is unstable, after the breaking of its CE with  $S_1$ ,  $Y_2$  will continuously decrease as  $x$  increases.



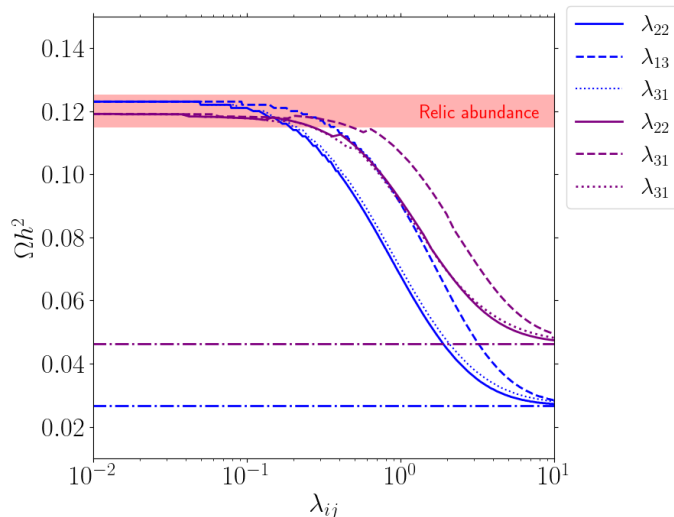


**Figure 4:** Relic abundance behavior as a function of the contact term couplings  $\lambda_{22}$ ,  $\lambda_{13}$  and  $\lambda_{31}$ . The solid, dashed and dotted lines are obtained with `darkOmegaN`, whereas the dashed-dot lines are obtained with `darkOmega`. The blue lines correspond to  $(m_1, m_2) = (500, 505)$  GeV and  $(\lambda_{H1}, \lambda_{12}, \lambda_{H2}) = (0, 2.6 \times 10^{-5}, 1)$ , whereas the purple lines correspond to  $(m_1, m_2) = (500, 510)$  GeV and  $(\lambda_{H1}, \lambda_{12}, \lambda_{H2}) = (0, 3.2 \times 10^{-5}, 1)$ . In each case,  $\lambda_{12}$  was fixed to obtain the correct relic abundance (red band) with `darkOmegaN` for vanishing contact couplings.

requires nearly degenerate masses of the new scalars, i.e.  $m_1 \lesssim m_2 < m_h/2$ . On the other hand, we have checked numerically that in order to obtain the correct relic abundance  $\lambda_{12}$  would be large enough to also recover CE within the dark sector, making cospattering ineffective unless  $\lambda_{H2} \gtrsim 1$ . However, searches of Higgs to invisible at the LHC have set limits on  $\Gamma(h \rightarrow S_2 S_2)$  [23], that translate into  $\lambda_{H2} \lesssim 10^{-2}$ . We have also checked that the inclusion of the contact terms does not change this result.

To summarize, we have presented the cBE for the system of  $S_1$  and  $S_2$ , and we have solve them making use of the `micrOMEGAs` code. The three regimes that we have distinguished, cospattering, mediator FO, and (co)annihilations, depend strongly on the parameters  $\Delta m$  and  $\lambda_{12}$ , with cospattering favoring  $\Delta m \ll (m_1, m_2)$  and  $\lambda_{12} \ll 1$ . Besides, on-shell (inverse) decay rates of  $S_2$  are very efficient to maintain CE for much smaller values of  $\lambda_{12}$  than in the case of off-shell decays. Contact terms are not essential to have cospattering, and we have seen that light DM is ruled-out by LHC bounds.

## 4 Phenomenology

In this section we discuss direct detection and big-bang nucleosynthesis (BBN) constraints, and the prospects of having LLP in the cospattering scenario.

## 4.1 Constraints

### 4.1.1 Direct detection

The stable DM particle  $S_1$  could be observed in direct detection experiments via the Higgs portal. This implies a bound on the effective DM-Higgs coupling [24]

$$\lambda_{H1} \lesssim \sqrt{\frac{4\pi m_h^4 m_1^2 \sigma_{LZ}}{f_N^2 m_n^4}}, \quad (4.1)$$

where  $\sigma_{LZ}$  denotes the upper bounds at 90% C.L. on the effective DM-nucleon scattering cross section obtained from the LZ experiment [25],  $f_N \approx 0.3$  the effective nucleon-Higgs coupling,  $m_n \approx 0.9$  GeV the nucleon mass, and  $m_h = 125$  GeV the SM Higgs mass.

As cospattering can be achieved for sufficiently small values of  $\lambda_{H1}$ , one could investigate the maximum values taken by this parameter without jeopardizing the relic abundance obtained by `darkOmegaN` at the same time being in the ballpark of those values that yield a strong enough signal to be searched in future direct detection experiments. Certainly,  $\lambda_{H1}$  can not take arbitrarily large values, otherwise CE is recovered by processes of the type  $1h \leftrightarrow 2h$ . To quantify the interplay among all these effects, in Fig. 4 we show the effect of  $\lambda_{H1}$  on the relic abundance, for  $m_1 = 90$  and 500 GeV,  $\Delta m = 1$  GeV and  $\lambda_{H2} = 1$ . Besides, the color indicates the value of  $\Delta_{1s}^\Omega$  (see eq. 3.5). As expected, sizable values of  $\lambda_{H1}$  decrease the relic abundance with respect to vanishing  $\lambda_{H1}$ , and for very large values of this parameter CE is recovered. However, LZ bounds (solid vertical lines) do not allow such sizable values of  $\lambda_{H1}$ , ruling out strong deviations from the co-scattering regime as given by `darkOmegaN`. In particular, for  $m_1 = 500$  GeV, it is possible to have sizable values of this parameter, i.e.  $\lambda_{H1} \sim 10^{-2}$ , in the ballpark of LZ bounds (but still evading them), and without recovering CE. Actually, in that specific case, Darwin experiments [26] will be sensitive to regions with even smaller values of  $\lambda_{H1}$  (dashed vertical lines in Fig. 4 (right)).

We point out that if loop corrections are considered, the DM-Higgs coupling should be renormalized on-shell in order to retain agreement with eq. (4.1) at higher orders. We have outlined a suitable treatment of loop corrections in appendix C and found that in our model the loop effects to the observables of interest are negligible.

### 4.1.2 BBN

Additional stable or decaying particles present at temperatures  $T \leq 10$  MeV may affect the measured primordial abundances of light elements. To our knowledge, constraints on lifetime of new singlet scalars have been only considered for masses  $\leq m_h/2$  [27]. We estimate the bounds coming from BBN using the results obtained in [28], considering the relic abundance of  $S_2$  before its decay and the branching fraction of decays of  $S_2$  into hadronic decays. In the present Higgs portal scenario, for  $\Delta m \gtrsim 1$  GeV the model is practically safe of BBN constraints in the parameter space that we explore, since just after the decoupling of  $S_2$  from the thermal plasma,  $\Omega_{S_2} h^2$  is at least one order of magnitude below the measured DM relic abundance. The same conclusions were obtained in the leptophilic DM scenario in the cospattering mechanism [7].

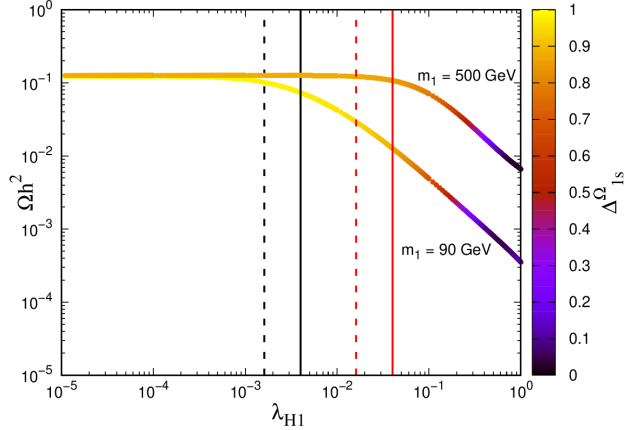


**Figure 5:** Relic abundance as a function of  $\lambda_{H1}$  considering  $\Delta m = 1$  GeV,  $\lambda_{H2} = 1$  and no contact terms. The vertical lines represent the bound from LZ [25] and DARWIN projections [26], with the black solid (black dashed) and red solid (red dashed) lines representing the upper bounds for  $m_1 = 90$  and 500 GeV, respectively.  $\lambda_{12}$  has been chosen such that observed relic density is satisfied in the co-scattering regime,  $\lambda_{12} = \{3.86 \times 10^{-4}, 2.3 \times 10^{-5}\}$  for  $m_1 = \{90, 500\}$  GeV respectively.

## 4.2 Long-lived particles

In the cospattering regime, the coupling  $\lambda_{12}$  which determines the decay width of  $S_2$  is very small, while simultaneously  $\Delta m \ll (m_1, m_2)$ . Therefore, the dark partner  $S_2$  typically constitutes a long-lived particle (LLP) with a wide range of possible lifetimes in different regions of the parameter space. While single production of  $S_2$  (like production of the DM relic  $S_1$ ) at colliders is suppressed by  $\lambda_{12}$ , pair production of  $S_2$  through an intermediate Higgs boson must be sizable, via the chain [29]

$$pp \rightarrow h^* + X \rightarrow S_2 + S_2 + X, \quad (4.2)$$

with  $X$  being other states not relevant for the discussion. The goal of this section is to compare a few  $S_2$  lifetime estimations predicted by the extended Higgs-singlet scenario that could be in the reach of present and future experiments, specially when the production mechanism is motivated by cospattering. In our knowledge, as LLP in Higgs portals have only been considered for mediator masses  $\lesssim m_h/2$  [14, 30], the results presented here could motivate the search of heavier scalars through the Higgs portal.

In Fig. 6, we show the results for the lifetime of  $S_2$  as a function of its mass for  $\lambda_{H1} = 0$  and fixed  $\lambda_{H2} = 0.5$  (left), 1 (middle) and  $\pi$  (right). The row of points from top to bottom corresponds to  $\Delta m = 1, 5, 10$  and 20 GeV, while the color of each point indicates  $\Delta_{1s}^\Omega$ . The variation in  $c\tau$  depends strongly on scalar mass difference, with small values of  $\Delta m$  favoring the cospattering regime ( $\Delta_{1s}^\Omega \lesssim 1$ ), and in turn giving rise to enormous lifetimes of  $S_2$ , with some of the points well beyond earth size experiments, thereby confronting bounds coming from BBN. As  $\Delta m$  increases, the values of  $c\tau$  decrease to the point of reaching typical decay lengths for future experiments such as MATHUSLA [14]. Notice that the reach of

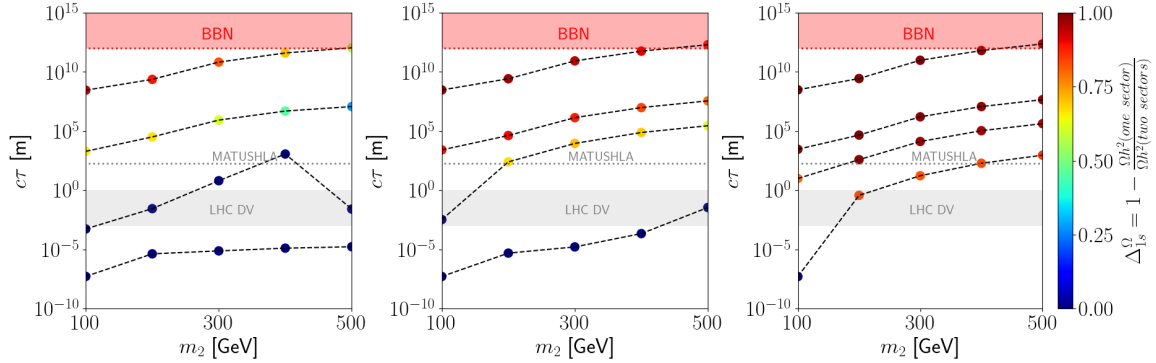


**Figure 6:** Proper lifetime of the mediator as a function of its mass in the SBS, for  $\lambda_{H2} = 0.5, 1$  and  $\pi$ , respectively, and  $\lambda_{12}$  fixed to obtain the correct relic abundance. In each plot, from top to bottom  $\Delta m = 1, 5, 10$  and  $20$  GeV, respectively. The color of each point represents the value of  $\Delta_{1s}^{\Omega}$ .

the latter may not only test particles that were produced in the cospattering regime, but also probe the other two regimes that we studied in Sec 3.2 (blue points). There are also model predictions in the reach of displaced vertex (DV) for ATLAS or CMS [31] (grey band in each plot). Finally, the blue points in each plot are not unique for the corresponding chosen parameter space points shown in Fig. 6, since as some of them belong to the mediator freeze-out regime (see region II in Fig. 2), there is a range of  $\lambda_{12}$  values fulfilling the measured relic abundance, then varying in orders of magnitude their corresponding  $c\tau$  value.

## 5 Conclusions

In this work, we have studied for the very first time the simplest Higgs portal scenario in the context of cospattering. This SM extensions considers two real scalars charged under a single  $Z_2$  discrete symmetry, in which after EWSB, the lightest eigenstate is cosmologically stable, and the heavier one is unstable. We have explored in major detail the impact of each parameter in the thermal mechanism: cospattering, mediator freeze-out, and DM freeze-out. We put special attention to the first case, identifying parameter space for DM and mediator masses of hundreds of GeV giving the correct relic abundance. Radiative corrections do not generate significant deviations to the results that we obtain neither in direct detection nor in the calculation of the relic abundance. Besides, we have shown that the cospattering regime for the extended singlet-Higgs scenario gives rise to (very)long-lived mediators that could be in the reach of present and future experiments. Finally, effects of early kinetic decoupling [32] on the relic calculation could modify at some extent the results presented in this work, but this analysis is beyond the scope of our work.

## Acknowledgments

We thank the creators and developers of `micrOMEGAs`, and a special thank to Sasha Pukhov for his constant assistance on `micrOMEGAs`. We thank Gael Alguero for providing important

information relevant to our work. We also thank Giovanna Cottin for helpful advice on the long-lived particle subject. B.D.S has been funded by ANID (ex CONICYT) Grant No. 3220566. B.D.S. and J.L want to thank DESY and the Cluster of Excellence Quantum Universe, Hamburg, Germany, where this work was initiated.

## A Lagrangian original basis

In this appendix we develop the details of the model in terms of the original field basis, which after some algebra becomes the simplified Lagrangian that we used in eq. 2.1.

Let us consider two real singlet scalars  $\tilde{S}_1$  and  $\tilde{S}_2$ , charged under the same  $Z_2$  symmetry such that  $X \rightarrow X$  and  $\tilde{S}_i \rightarrow -\tilde{S}_i$ , with  $i = 1, 2$  [16, 17]. The corresponding potential is given by

$$V(H, S_1, S_2) \supset \tilde{m}_1^2 \tilde{S}_1^2 + \tilde{m}_2^2 \tilde{S}_2^2 + \tilde{\lambda}_{H1} \tilde{S}_1^2 H^\dagger H + \tilde{\lambda}_{12} \tilde{S}_1 \tilde{S}_2 H^\dagger H + \tilde{\lambda}_{H2} \tilde{S}_2^2 H^\dagger H + \tilde{\lambda}_{22} \tilde{S}_1^2 \tilde{S}_2^2 + \tilde{\lambda}_{13} \tilde{S}_1 \tilde{S}_2^3 + \tilde{\lambda}_{31} \tilde{S}_1^3 \tilde{S}_2. \quad (\text{A.1})$$

After EWSB, with  $\langle H \rangle = (0, v_h)^T / \sqrt{2}$ , the scalars  $\tilde{S}_1$  and  $\tilde{S}_2$  mix, but after rotation the potential can be written identically as in A.1. We diagonalize using

$$O^T \mathcal{M}^2 O = \text{diag}(m_1^2, m_2^2) \quad (\text{A.2})$$

The mass matrix is

$$\mathcal{M}^2 = \begin{pmatrix} \tilde{m}_1^2 + \tilde{\lambda}_{H1} v_h^2 & \tilde{\lambda}_{12} v_h^2 / 2 \\ \tilde{\lambda}_{12} v_h^2 / 2 & \tilde{m}_2^2 + \tilde{\lambda}_{H2} v_h^2 \end{pmatrix} \quad (\text{A.3})$$

The Eigenmass are given by

$$m_1^2 = (\tilde{m}_1^2 + \tilde{\lambda}_{H1} v_h^2) \cos^2 \theta + (\tilde{m}_2^2 + \tilde{\lambda}_{H2} v_h^2) \sin^2 \theta - \sin \theta \cos \theta \tilde{\lambda}_{12} v_h^2 \quad (\text{A.4})$$

$$m_2^2 = (\tilde{m}_2^2 + \tilde{\lambda}_{H2} v_h^2) \cos^2 \theta + (\tilde{m}_1^2 + \tilde{\lambda}_{H1} v_h^2) \sin^2 \theta + \sin \theta \cos \theta \tilde{\lambda}_{12} v_h^2 \quad (\text{A.5})$$

Additionally, from the non-diagonal relationship of eq. A.2 we obtain that

$$\tan(2\theta) = -\frac{\tilde{\lambda}_{12} v_h^2}{2(\tilde{m}_1^2 - \tilde{m}_2^2 + v_h^2(\tilde{\lambda}_{H1} - \tilde{\lambda}_{H2}))} \quad (\text{A.6})$$

Replacing eq. A.6 into the original Lagrangian, and writing down eq. A.1 in terms of the physical states, i.e.  $\tilde{S}_1 = \cos \theta S_1 + \sin \theta S_2$  and  $\tilde{S}_2 = -\sin \theta S_1 + \cos \theta S_2$ , we obtain the potential presented in eq. 2.1.

## B Dark Matter Conversion Rate

In this section we present a calculation of the thermally averaged cross section for DM conversion  $\langle \sigma_{2X \rightarrow 1X v} \rangle$  where  $X$  can be any SM particle. The differential cross section of the conversion process in the centre of mass frame is given by

$$\left( \frac{d\sigma_{2X \rightarrow 1X v}}{d\Omega} \right)_{c.o.m.} = \frac{|\mathbf{p}_f|}{64\pi^2 E_2 E_X \sqrt{s}} |\overline{\mathcal{M}}|_{2X \rightarrow 1X}^2, \quad (\text{B.1})$$

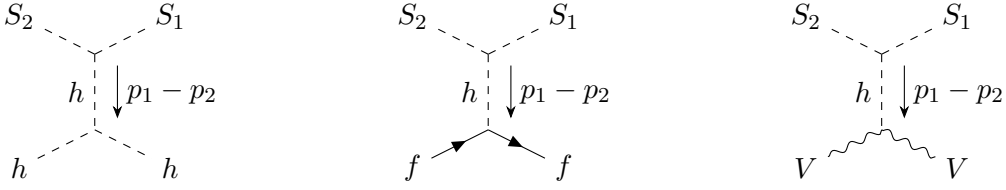


**Figure 7:** Tree-level contributions to  $S_2 \rightarrow S_1$  conversions in the thermal bath.

where  $\sqrt{s}$  denotes the total c.o.m. energy,  $|\mathbf{p}_f| = \lambda(s, m_1^2, m_X^2)^{1/2}/(2\sqrt{s})$  denotes the final state momentum<sup>5</sup> and  $E_2 = (|\mathbf{p}_i|^2 + m_2^2)^{1/2}$  and  $E_X = (|\mathbf{p}_i|^2 + m_X^2)^{1/2}$  denote the energies of the initial state DM and SM particle with momentum  $|\mathbf{p}_i| = \lambda(s, m_2^2, m_X^2)^{1/2}/(2\sqrt{s})$ . At tree-level the conversion processes are possible for  $X = h, f, W, Z$  through the  $t$ -channel diagrams shown in Fig. 7. The resulting squared matrix elements are given by

$$\overline{|\mathcal{M}|}_{2h \rightarrow 1h}^2 = \frac{9\lambda_{12}^2 m_h^4}{(t - m_h^2)^2}, \quad (\text{B.2a})$$

$$\overline{|\mathcal{M}|}_{2f \rightarrow 1f}^2 = \frac{2\lambda_{12}^2 m_f^2 (4m_f^2 - t)}{(t - m_h^2)^2}, \quad (\text{B.2b})$$

$$\overline{|\mathcal{M}|}_{2V \rightarrow 1V}^2 = \frac{4\lambda_{12}^2 m_V^2 (3m_V^2 + t)}{(t - m_h^2)^2}, \quad (\text{B.2c})$$

where

$$t = (p_1 - p_2)^2 = 2m_X^2 - 2(|\mathbf{p}_i|^2 + m_X^2)^{1/2}(|\mathbf{p}_f|^2 + m_X^2)^{1/2} + 2|\mathbf{p}_f||\mathbf{p}_i|\cos\theta. \quad (\text{B.3})$$

After substitution, the solid angle differential becomes  $d\Omega = d\varphi dt / (2|\mathbf{p}_f||\mathbf{p}_i|)$  and the integrals can be solved to obtain the total cross section

$$\sigma_{2h \rightarrow 1h\nu} = \frac{9\lambda_{12}^2 m_h^4 |\mathbf{p}_f|}{16\pi E_2 E_X \sqrt{s}} \frac{1}{(m_h^2 - t^-)(m_h^2 - t^+)}, \quad (\text{B.4a})$$

$$\sigma_{2f \rightarrow 1f\nu} = \frac{\lambda_{12}^2 m_f^2}{32\pi E_2 E_X |\mathbf{p}_i| \sqrt{s}} \left[ \ln\left(\frac{m_h^2 - t^-}{m_h^2 - t^+}\right) - \frac{4|\mathbf{p}_i||\mathbf{p}_f|(m_h^2 - 4m_f^2)}{(m_h^2 - t^-)(m_h^2 - t^+)} \right], \quad (\text{B.4b})$$

$$\sigma_{2V \rightarrow 1V\nu} = \frac{\lambda_{12}^2 m_V^2}{16\pi E_2 E_X |\mathbf{p}_i| \sqrt{s}} \left[ \frac{4|\mathbf{p}_i||\mathbf{p}_f|(m_h^2 + 3m_V^2)}{(m_h^2 - t^-)(m_h^2 - t^+)} - \ln\left(\frac{m_h^2 - t^-}{m_h^2 - t^+}\right) \right], \quad (\text{B.4c})$$

where  $t^\pm \equiv t(\cos\theta = \pm 1)$ . Next, the thermal average has to be calculated from

$$\langle \sigma v \rangle = \int_{(m_2 + m_X)^2}^{\infty} \frac{E_2 E_X \sigma v}{4m_2^2 m_X^2 T} \frac{K_1(\frac{\sqrt{s}}{T})}{K_2(\frac{m_2}{T}) K_2(\frac{m_X}{T})} \sqrt{s - 2(m_2^2 + m_X^2) + \frac{(m_2^2 - m_X^2)^2}{s}}. \quad (\text{B.5})$$

To good approximation, this integral is given by  $\langle \sigma v \rangle \approx \sigma v(s = \langle s \rangle)$  where

$$\langle s \rangle \approx (m_2 + m_X)^2 + 6(m_2 + m_X)T + \mathcal{O}(T^2/m_2^2), \quad (\text{B.6})$$

<sup>5</sup> $\lambda(x, y, z) = (x - y - z)^2 - 4yz$  is the Källén function.

such that the thermally averaged cross sections, in the limit  $T, \Delta m \ll m_{1,2}$ , are given by

$$\langle \sigma_{2h \rightarrow 1hv} \rangle \approx \frac{9\lambda_{12}^2}{8\pi} \sqrt{\frac{\Delta m + 3T}{2m_2 m_h (m_2 + m_h)^3}} \quad (\text{B.7a})$$

$$\langle \sigma_{2f \rightarrow 1fv} \rangle \approx \frac{\lambda_{12}^2 m_f^4}{\pi m_h^4} \sqrt{\frac{\Delta m + 3T}{2m_2 m_f (m_2 + m_f)^3}} \quad (\text{B.7b})$$

$$\langle \sigma_{2V \rightarrow 1Vv} \rangle \approx \frac{3\lambda_{12}^2 m_V^4}{2\pi m_h^4} \sqrt{\frac{\Delta m + 3T}{2m_2 m_V (m_2 + m_V)^3}} \quad (\text{B.7c})$$

Finally, the DM conversion rate is  $\Gamma_{1 \rightarrow 2} = (n_2^e/n_1^e) \sum_X \langle \sigma_{2X \rightarrow 1Xv} \rangle n_X^e$ .

### C Treatment of Radiative Corrections



**Figure 8:** Schematic diagrams showing the contribution of the effective DM-Higgs vertex  $\lambda_{DM}(q^2)$  to direct detection (left) and coannihilation processes during freeze-out (right).

In this appendix we outline the on-shell renormalization of the model and estimate the impact of one-loop corrections on the results obtained in this paper. We note that a proper definition of the renormalization conditions is crucial in order to obtain meaningful results at NLO. In particular, the physical interpretation of the parameters at tree-level is only retained if they fulfill corresponding on-shell renormalization conditions at one-loop order. In other schemes like  $\overline{MS}$  or for ad-hock subtractions the model parameters no longer correspond directly to the observables of interest. The parameters relevant for a renormalization of the scalar sector are the scalar masses  $m_i^2$ , quartic couplings  $\lambda_{ij}$  and Higgs vev  $v_h$ . The renormalized Lagrangian is obtained from the following renormalization transformation of the bare parameters

$$m_{i,0}^2 \rightarrow m_i^2 + \delta m_i^2, \quad \lambda_{ij}^0 \rightarrow \lambda_{ij}^R + \delta \lambda_{ij}, \quad v_h^0 \rightarrow v_h + \delta v_h, \quad (\text{C.1})$$

and renormalization of the bare fields

$$S_i^0 \rightarrow \sqrt{Z_i} S_i, \quad H_0 \rightarrow \sqrt{Z_H} H, \quad \text{where } Z_i = 1 + \delta Z_i. \quad (\text{C.2})$$

After on-shell renormalization, the scalar masses  $m_i$  correspond to the physical pole masses of the DM particles and the scalar couplings  $\lambda_{ij}^R$  correspond to physical effective coupling strengths measured e.g. in direct detection or collision experiments. This implies a set of conditions on the corresponding amplitudes from which the renormalization constants can be determined. Here, we demonstrate this specifically for  $\lambda_{H1}$  and  $\lambda_{12}$ , which where

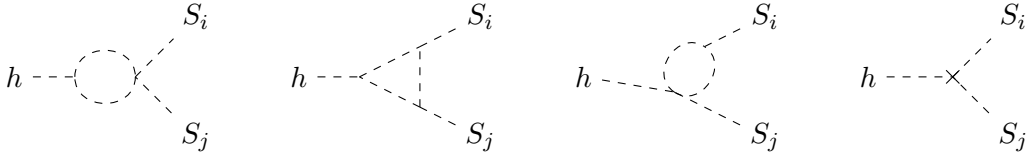


**Figure 9:** Diagrams contributing to  $h \rightarrow S_i S_j$  at one-loop order.

chosen to be very small in the above analysis. We define  $\lambda_{H1}$  to be the effective  $S_1$ -Higgs coupling measured in the direct detection experiments sketched in Fig. 8 (left), while  $\lambda_{12}$  is defined through DM production and annihilation events at  $\langle s \rangle = (m_1 + m_2)^2$  such as in Fig. 8 (right). Note that, in general, the effective (quantum corrected) DM-Higgs couplings denoted by  $\lambda_{ij}(q^2)$  will be dependent on the (off-shell) Higgs momentum  $q$ . At one-loop these effective couplings are given by

$$\lambda_{H1}(q^2) = \lambda_{H1}^R + \Gamma_{H1}(q^2) + \delta\lambda_{H1} + \lambda_{H1}^R \left( \delta Z_1 + \frac{1}{2} \delta Z_H + \frac{\delta v_h}{v_h} \right) \quad (\text{C.3a})$$

$$\lambda_{12}(q^2) = \lambda_{12}^R + \Gamma_{12}(q^2) + \delta\lambda_{12} + \lambda_{12}^R \left( \frac{1}{2} \delta Z_1 + \frac{1}{2} \delta Z_2 + \frac{1}{2} \delta Z_H + \frac{\delta v_h}{v_h} \right) \quad (\text{C.3b})$$

where  $\Gamma_{ij}(q^2)$  denotes the contributions of the one-loop diagrams from Fig. 9. The definitions of the coupling strengths translate into the following renormalization conditions

$$\lambda_{H1}^R \equiv \lambda_{H1}(0), \quad \lambda_{12}^R \equiv \lambda_{12}(\langle s \rangle) \quad (\text{C.4})$$

And can easily be fulfilled by choosing the renormalization constants  $\delta\lambda_{H1}$  and  $\delta\lambda_{12}$  appropriately. In the limit  $\lambda_{H1}^R, \lambda_{12}^R \approx 0$  the only contributing one-loop diagrams are of the type Fig. 9 (left) and result in the following expressions for the renormalized vertex functions

$$\lambda_{H1}(q^2) = \lambda_{H1}^R - \frac{\lambda_{22}^R \lambda_{H2}^R}{8\pi^2} \left( B_0(q^2, m_2^2, m_2^2) - B_0(0, m_2^2, m_2^2) \right) \quad (\text{C.5})$$

$$\lambda_{12}(q^2) = \lambda_{12}^R - \frac{3\lambda_{13}^R \lambda_{H2}^R}{16\pi^2} \left( B_0(q^2, m_2^2, m_2^2) - B_0(\langle s \rangle, m_2^2, m_2^2) \right) \quad (\text{C.6})$$

By definition of the on-shell scheme, quantum corrections to direct detection of  $S_1$  and to annihilation and production processes of  $S_1 + S_2$  during freeze-out are 0. Corrections only appear for annihilation and production of  $S_1$ , where the relevant momentum transfer is  $q^2 = 4m_1^2$ . The resulting effective coupling that should be used when calculating the relic abundance is (for  $m_1 \simeq m_2$ )

$$\lambda_{H1}(4m_1^2) \approx \lambda_{H1}^R - \frac{\lambda_{22}^R \lambda_{H2}^R}{4\pi^2} \quad (\text{C.7})$$

The loop corrections, as expected, result in very small  $\mathcal{O}(1\%)$  effects and do not have any important impact on the above analysis.

## References

- [1] R.T. D’Agnolo, D. Pappadopulo and J.T. Ruderman, *Fourth Exception in the Calculation of Relic Abundances*, *Phys. Rev. Lett.* **119** (2017) 061102 [1705.08450].



- [2] M. Garny, J. Heisig, B. Lülff and S. Vogl, *Coannihilation without chemical equilibrium*, *Phys. Rev. D* **96** (2017) 103521 [[1705.09292](#)].
- [3] H.-C. Cheng, L. Li and R. Zheng, *Coscatting/Coannihilation Dark Matter in a Fraternal Twin Higgs Model*, *JHEP* **09** (2018) 098 [[1805.12139](#)].
- [4] M. Garny, J. Heisig, M. Hufnagel and B. Lülff, *Top-philic dark matter within and beyond the WIMP paradigm*, *Phys. Rev. D* **97** (2018) 075002 [[1802.00814](#)].
- [5] R.T. D’Agnolo, C. Mondino, J.T. Ruderman and P.-J. Wang, *Exponentially Light Dark Matter from Coannihilation*, *JHEP* **08** (2018) 079 [[1803.02901](#)].
- [6] F. Brümmer, *Coscatting in next-to-minimal dark matter and split supersymmetry*, *JHEP* **01** (2020) 113 [[1910.01549](#)].
- [7] S. Junius, L. Lopez-Honorez and A. Mariotti, *A feeble window on leptophilic dark matter*, *JHEP* **07** (2019) 136 [[1904.07513](#)].
- [8] R.T. D’Agnolo, D. Pappadopulo, J.T. Ruderman and P.-J. Wang, *Thermal Relic Targets with Exponentially Small Couplings*, *Phys. Rev. Lett.* **124** (2020) 151801 [[1906.09269](#)].
- [9] M. Garny and J. Heisig, *Bound-state effects on dark matter coannihilation: Pushing the boundaries of conversion-driven freeze-out*, *Phys. Rev. D* **105** (2022) 055004 [[2112.01499](#)].
- [10] J. Herms and A. Ibarra, *Production and signatures of multi-flavour dark matter scenarios with  $t$ -channel mediators*, *JCAP* **10** (2021) 026 [[2103.10392](#)].
- [11] J. Heeck, J. Heisig and A. Thapa, *Dark matter and radiative neutrino masses in conversion-driven scotogenesis*, *Phys. Rev. D* **107** (2023) 015028 [[2211.13013](#)].
- [12] A. Filimonova, S. Junius, L. Lopez Honorez and S. Westhoff, *Inelastic Dirac dark matter*, *JHEP* **06** (2022) 048 [[2201.08409](#)].
- [13] J. Heisig, A. Lessa and L.M.D. Ramos, *Probing conversion-driven freeze-out at the LHC*, [2404.16086](#).
- [14] D. Curtin et al., *Long-Lived Particles at the Energy Frontier: The MATHUSLA Physics Case*, *Rept. Prog. Phys.* **82** (2019) 116201 [[1806.07396](#)].
- [15] G. Cottin, *LLP overview: theory perspective*, *PoS LHCP2023* (2024) 164.
- [16] K. Ghorbani and H. Ghorbani, *Scalar split WIMPs in future direct detection experiments*, *Phys. Rev. D* **93** (2016) 055012 [[1501.00206](#)].
- [17] J.A. Casas, D.G. Cerdeño, J.M. Moreno and J. Quilis, *Reopening the Higgs portal for singlet scalar dark matter*, *JHEP* **05** (2017) 036 [[1701.08134](#)].
- [18] G. Belanger, F. Boudjema, A. Pukhov and A. Semenov, *MicrOMEGAs: A Program for calculating the relic density in the MSSM*, *Comput. Phys. Commun.* **149** (2002) 103 [[hep-ph/0112278](#)].
- [19] G. Alguero, G. Belanger, S. Kraml and A. Pukhov, *Co-scattering in micrOMEGAs: a case study for the singlet-triplet dark matter model*, [2207.10536](#).
- [20] B. Díaz Sáez, K. Möhling and D. Stöckinger, *Two real scalar WIMP model in the assisted freeze-out scenario*, *JCAP* **10** (2021) 027 [[2103.17064](#)].
- [21] G. Belanger and J.-C. Park, *Assisted freeze-out*, *JCAP* **1203** (2012) 038 [[1112.4491](#)].
- [22] T.N. Maity and T.S. Ray, *Exchange driven freeze out of dark matter*, *Phys. Rev. D* **101** (2020) 103013 [[1908.10343](#)].

- [23] ATLAS collaboration, *Search for invisible Higgs-boson decays in events with vector-boson fusion signatures using  $139 \text{ fb}^{-1}$  of proton-proton data recorded by the ATLAS experiment*, *JHEP* **08** (2022) 104 [[2202.07953](#)].
- [24] J.M. Cline, K. Kainulainen, P. Scott and C. Weniger, *Update on scalar singlet dark matter*, *Phys. Rev. D* **88** (2013) 055025 [[1306.4710](#)].
- [25] LZ collaboration, *First Dark Matter Search Results from the LUX-ZEPLIN (LZ) Experiment*, *Phys. Rev. Lett.* **131** (2023) 041002 [[2207.03764](#)].
- [26] DARWIN collaboration, *DARWIN: towards the ultimate dark matter detector*, *JCAP* **11** (2016) 017 [[1606.07001](#)].
- [27] A. Fradette and M. Pospelov, *BBN for the LHC: constraints on lifetimes of the Higgs portal scalars*, *Phys. Rev. D* **96** (2017) 075033 [[1706.01920](#)].
- [28] K. Jedamzik, *Big bang nucleosynthesis constraints on hadronically and electromagnetically decaying relic neutral particles*, *Phys. Rev. D* **74** (2006) 103509 [[hep-ph/0604251](#)].
- [29] N. Craig, H.K. Lou, M. McCullough and A. Thalappilil, *The Higgs Portal Above Threshold*, *JHEP* **02** (2016) 127 [[1412.0258](#)].
- [30] J. Alimena et al., *Searching for long-lived particles beyond the Standard Model at the Large Hadron Collider*, *J. Phys. G* **47** (2020) 090501 [[1903.04497](#)].
- [31] L. Lee, C. Ohm, A. Soffer and T.-T. Yu, *Collider Searches for Long-Lived Particles Beyond the Standard Model*, *Prog. Part. Nucl. Phys.* **106** (2019) 210 [[1810.12602](#)].
- [32] T. Binder, T. Bringmann, M. Gustafsson and A. Hryczuk, *Early kinetic decoupling of dark matter: when the standard way of calculating the thermal relic density fails*, *Phys. Rev. D* **96** (2017) 115010 [[1706.07433](#)].